TRACING CURVILINEAR STRUCTURES IN LIVE CELL IMAGES

M. E. Sargın, A. Altınok, K. Rose, B. S. Manjunath

Dept. of Electrical and Computer Engineering,
University of California Santa Barbara, Santa Barbara, CA 93106
{msargin,alphan,rose,manj}@ece.ucsb.edu

ABSTRACT

Tracing of curvilinear structures is one of the fundamental tools in the quantitative analysis of biological images, for extracting information about structures such as blood vessels, neurons, microtubules, and similar entities. Due to the limitations in biological sample preparation and fluorescence imaging, typical images in live cell studies exhibit severe noise and considerable clutter. These images are manually analyzed through a laborious and approximate set of quantification tasks. In this paper, we describe a constrained optimization method for extracting curvilinear structures from live cell fluorescence images. We show that the proposed method is largely insensitive to frequent intersections, intensity variations along the curve, and generates successful traces within noisy regions. We demonstrate the results of our approach on live cell microtubule images.

***Index Terms*—** Biomedical image processing, biomedical measurements

1. INTRODUCTION

In this work, we propose a robust curve tracing algorithm that is insensitive to problems frequently encountered in fluorescence live cell images. Typically, these images exhibit *high clutter*, such as frequent intersections and overlaps, with occasional loss of signal along the curve appearing as *gaps*, and high levels of noise due to *sample fluorescence*. A number of potential applications exist in the analysis of biological structures from images, such as blood vessels, neurons, and microtubules. Live cell studies rely on fluorescence imaging, which presents atypical challenges for the analysis of these images, Sec.1.1. We propose a constrained optimization method for tracing curvilinear structures in severe noise and clutter. A directional constraint is imposed on the optimization step that minimizes the difference between the recorded image and the best model-based approximation of it. We provide results on actual microtubule images.

The rest of this paper is organized as follows. Next, we briefly describe microtubules, related research, and the associated imaging and analysis problems. In Section 2, we review related work. In Section 3, we describe the proposed method. In Section 4, we provide experimental results. In Section 5, we discuss our tracing method and results.

This study was funded by Center for Bioimage Informatics under grants NSF-ITR 0331697.

1.1. Analysis of Microtubule Dynamics in Live Cell Image Sequences

Microtubules (MTs) are filamentous cytoskeletal structures composed of tubulin protein subunits. These subunits can add on, or dissociate from, the tubulin polymer rapidly, making MTs highly dynamic. Through these dynamic behaviors, MTs are critically involved in many essential cellular functions, [1].

To obtain a quantitative description of MT behavior under different experimental conditions, researcher track individual MT tips from time lapse images of live cell MTs, Fig.1. Traditional MT dynamics parameters quantify statistics derived from the *growth* and *shortening* events between consecutive frames.

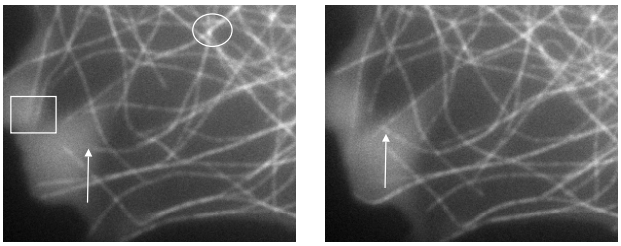

(a) (b)

Fig. 1. Consecutive time-lapse images of MTs taken at 4 sec. intervals. Marked MT (arrow) grows in length. Oval region shows increased fluorescence at intersections. Rectangular region is an example of high levels of noise.

Live cell MTs are imaged using fluorescence microscopy. A particular problem of this technique is the sample fluorescence that severely degrades the image contrast and results in uneven illumination levels due to non-uniform distribution of MTs. For example, high concentrations of the fluorescent protein subunits cause considerable haze around the MTs, Fig.1. Note that sample fluorescence causes consid-

erable signal degradation in addition to the one introduced by the imaging equipment. Furthermore, frequent intersections and overlaps cause intensity variations along the MT body. Thus, typically only a few MTs are selected for manual tracking which potentially provides a limited representation of underlying dynamic behavior. For instance, while different subsets of MTs undertake distinct tasks in the cell, and therefore can exhibit distinct dynamic characteristics, generally there are limited means of observing such dynamics in isolation through manual methods.

2. RELATED WORK

A number of tracing algorithms were proposed for extracting curvilinear structures from images, such as the anisotropic Gauss filtering, differential geometric properties of images [2], and using active contour approaches [3]. In [4], the authors propose a curvature-guided technique for tracing curves. [5] improves upon [2] by constraining the linking procedure of curve segments. Other examples include, region growing [6], derivations of active contours, and the level set methods [7]. Most tracing algorithms are swayed by frequent intersections and local variations of intensity along the curves. For example, Fast Marching prefers higher intensity levels using the geodesic distance, Fig.5(c), and does not use direction information along the curve. Thus, any neighboring structure could steal the trace.

Sample fluorescence is solely dependent upon the distribution of biological structures and generally is not adequately addressed by conventional techniques such as deconvolution. Tracing algorithms that use intensity information are sensitive to variations along the curve, which is the typical case in live cell images. Methods that are based on local gradient information often fail when reliable gradients cannot be computed around intersections. Segmental traces often fail when extracting individual segments within the regions of dense intersections becomes unreliable.

3. METHOD

In particular, our tracing algorithm addresses frequent intersections, gaps, and noise around the structure. The key idea is to propagate the trace from an initial point on the curve in all directions and select the best trace whose convolution with a kernel, representing the distortion, approximates the observation. For a given starting point on the structure, all possible paths can be represented by a graph (tree) with a branching factor of 8, where the vertices correspond to image pixels and the edges correspond to the directional weights. Then, the trace can be evaluated as the path from the root node to a leaf node optimizing a criterion. However, the computational cost of building the full graph is prohibitive.

We impose the following constraints on the construction of the graph. Instead of examining all directions, in each step we consider the best k candidate directions satisfying a threshold on the second derivative along the normal to the estimated local trace direction, Fig.2.

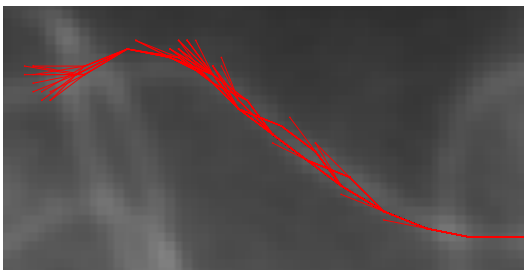

Fig. 2. Iteratively constructed paths along the curve.

Candidates of the best direction provide considerable computational savings as well as a stopping condition for the trace, e.g. determining the leaf nodes. Since the degenerate case of evaluating immediate neighbors in each step could cause the trace to terminate unexpectedly due to gaps along the curve, we consider candidates d pixels away from the previous node. This provides additional savings in computational cost by limiting the depth of the graph.

Note that the extracted paths are binary estimates of the curve being traced. In selecting the best path, we consider the imaging distortion and minimize the error between the observation, $O(x, y)$, and the convolution of each binary path, $B_i(x, y)$, with a variable kernel, $K_i(x, y)$, representing the distortion on the trace.

3.1. Construction of candidate paths

We construct the space of source paths as follows. Since local gradient information is highly sensitive to intersections, gaps and noise, we predict the direction at every iteration based on the previous trace points, and examine a neighborhood for best candidate directions computed along the normal.

Let $\mathbf{H}$ denote the Hessian at point (x_s, y_s). Then, the eigenvectors of $\mathbf{H}$ corresponding to the maximum and the minimum absolute eigenvalues will give the normal $(\mathbf{v_n})$ and parallel $(\mathbf{v_p})$ directions along the curve, respectively, [4, 6]. In the absence of previous trace points, we start to extend the curve $\mathcal{C}_i$ in $\mathbf{v_n}$ and $-\mathbf{v_n}$, otherwise the previous trace direction is taken as the initial estimate of the direction at that step. In every step, we consider pixels (x', y'), that are d apart from the last trace point (x_s, y_s),

$$(x', y') = (x_s, y_s) + d\mathbf{v_p}^T \tag{1}$$

Depending on the curvature at (x_s, y_s), the estimated position of the next curve point, (x', y'), may not be on the curve. Therefore, it should be projected back onto the curve. We consider a $(-\alpha, +\alpha)$ neighborhood of $(\mathbf{v_n})$ from the previous step as follows. Consider $\mathbf{v_n}$ on the points $\{(x', y') + d_c\mathbf{v_n}^T\}$,

where $d_c \in [-d, d]$. Then the $d_c^* > \tau$ are the candidate directions for trace propagation, where τ is a global threshold. Effectively, only those points that satisfy the threshold on the second directional derivative along $\mathbf{v_n}$ are added to the graph. If no candidate meets τ then the current node is assigned as a leaf node.

The line profile suggests that the first order derivative along $\mathbf{v_n}$ should also vanish at the center of the line. Therefore, fine refinement with sub-pixel accuracy can be applied. Approximating the image with Taylor series up to second order terms at $(x', y') + d_c^* \mathbf{v_n}^T$ and equating the directional derivative along $\mathbf{v_n}$ to zero yields,

$$d_f^* = -\frac{\mathbf{v_n}^T \nabla O(x,y)}{\mathbf{v_n}^T \mathbf{H} \mathbf{v_n}} \tag{2}$$

Finally, the total refinement d_t^* will be $d_c^* + d_f^*$.

An example graph constructed along the curve is shown in Fig.2. By evaluating paths on this graph, we can optimize the sum of local directions of a trace to conform with the observation.

3.2. Selecting the best path

Each $\mathcal{C}_i$ is constructed by traversing the graph from the root node to each leaf node. Associated cost between the observation image $O(x, y)$ and estimated source paths $\mathcal{C}_i$ are given by

$$f_i(\kappa_i) = \sum_{x,y} |O(x,y) - B_i(x,y) * K_i(x,y)|^2 \tag{3}$$

where $K_i(x, y)$ is the convolution kernel that approximates the combined effects of fluorescence emission and imaging equipment. An inverse squared kernel, $K_i(x, y) = \kappa_i/(1 + x^2 + y^2)$, imitating the light propagation, or any log-concave (e.g. Gaussian) PSF estimate of the imaging device are suitable kernels. Due to the fact that the resolution of the imaging device is too coarse to detect individual fluorophore molecules, the intensity observed at each pixel will reflect the density of fluorophore molecules within that specific pixel. Further, $B_i(x, y)$ denotes the binary image formed by the superposition of the indicator functions $I(x_i^j, y_i^j)$ for all n_i points in each path $\mathcal{C}_i$,

$$B_i(x,y) = \sum_{j=1}^{n_i} I(x_{i,j}, y_{i,j}) \tag{4}$$

where, $\mathcal{C}_i$ represents the i^{th} curve consists of ordered 8-connected points

$$\mathcal{C}_i = \{(x_{i,1}, y_{i,1}), \ldots, (x_{i,n_i}, y_{i,n_i})\}. \tag{5}$$

3.2.1. *Determination of* κ_i

Once we have completed the tracing for $\mathcal{C}_i$, we find the corresponding center value of the kernel, κ_i, by optimizing the cost function $f_i(\kappa_i)$. The κ_i^* that minimizes $f_i(\kappa_i)$ is given by

$$\kappa_i^* = \frac{\sum_{x,y}(B(x,y) * K^1(x,y))O(x,y)}{\sum_{x,y}(B(x,y) * K^1(x,y))^2}, \tag{6}$$

where $K^1(x, y)$ is the $K(x, y)$ with $\kappa = 1$. Having obtained the optimal cost function $f_i(\kappa_i^*)$ for all paths, the best path is then determined as the path that minimizes the optimal cost function over all set of paths.

$$\mathcal{C}^* = \underset{i}{\operatorname{argmin}}\, f_i(\kappa_i^*) \tag{7}$$

4. EXPERIMENTAL RESULTS

In evaluating our method, we traced MTs in live cell images obtained from [8]. The ability of tracking individually selected MTs is ultimately important for biological research. Thus, an initial point on the curve is manually selected and initial propagation directions are determined by the eigenvectors of $\mathbf{H}$, $(\mathbf{v_n})$ and $(\mathbf{v_p})$. The average width of MTs was determined as approximately 3 pixels. Application specific parameter values were found to be $d = 5$ and $k = 3$. Fig.3 shows the resulting traces on a toy example.

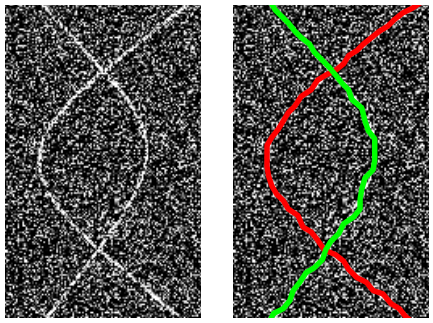

(a) (b)

Fig. 3. Example run on a synthetic image.

Fig.5 shows the resulting traces on actual MT images. In all cases, estimated traces successfully handled intersection points and intensity variations along the curve, despite the noise.

We evaluated our algorithm for its effectiveness to handle intersections. 100 intersections were randomly chosen, out of which we counted the number of correct handling. In some cases, encountered intersections were found to be too ambiguous to decide the direction of the trace for human vision as well, Table 1.

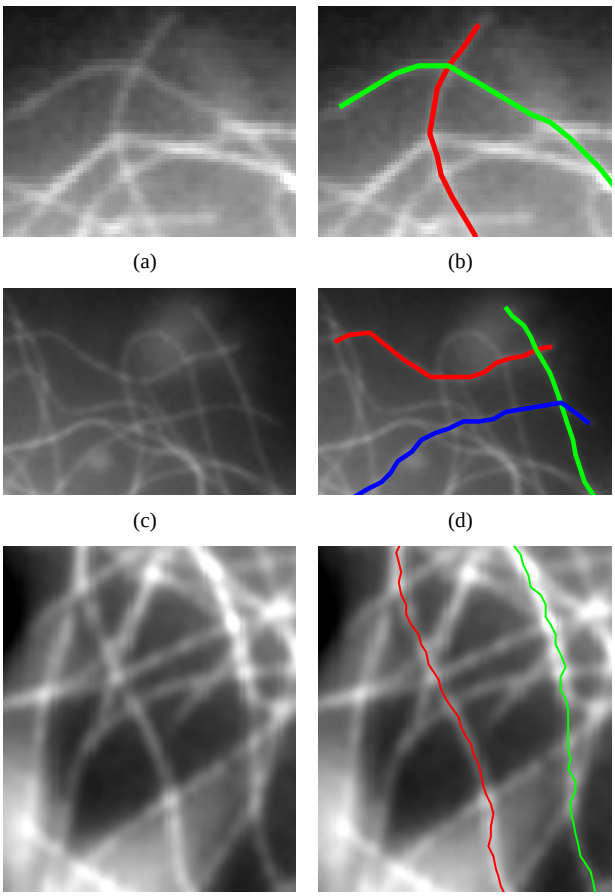

Fig. 4. Original regions with intersecting MTs (a,c,e), and corresponding traces (b,d,f).

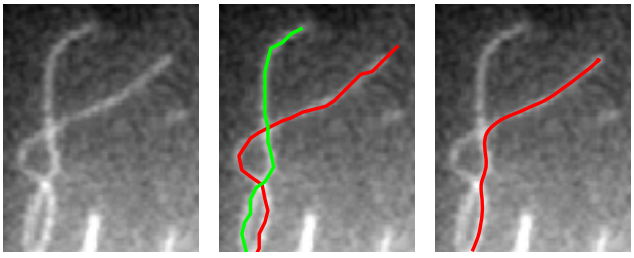

Fig. 5. Original region with intersecting MTs (a), and corresponding traces (b). Example Fast Marching trace favoring shorter geodesic distance and overlooking intersections.

Correct	Incorrect	Ambiguous
88	6	6

Table 1. Results of the proposed algorithm on handling the intersections.

5. CONCLUSION

The most noteworthy contribution of the proposed algorithm is the selection of the best trace from a set of candidate traces. Note that the kernel is adaptive and is optimized per trace. It is expected that not all points of the trace would lie exactly on the curve because of the step size. This is necessary for skipping gaps. However, the resulting trace points could easily be adjusted to the curve with a postprocessing step.

Clearly, initial seed points can be automatically determined independent of the algorithm. In the manual case, resulting traces do not depend on the initial point selection, provided that the initial point is not on a gap or intersection, potentially due to the initial propagation based on $\mathbf{H}$.

Finally, savings in computational cost can be given in terms of the step size, d, and the depth of the graph, D_G, as $O(1/d^{D_G})$. For example, the graph contains only $1/(5^{10})$ of all possible nodes with a step size of 5 pixels at depth 10.

6. ACKNOWLEDGEMENTS

We would like to thank Leslie Wilson and Stuart Feinstein for providing images and inspiring discussions on microtubule dynamics and the biological significance extracted features and correlations, as well as on image acquisition.

7. REFERENCES

[1] B. Alberts, A. Johnson, J. Lewis, M. Raff, K. Roberts, and P. Walter, *Molecular Biology of the Cell*, Garland Scientific, 4th edition edition, 2002.

[2] C. Steger, "An unbiased detector of curvilinear structures," *IEEE Transactions on Pattern Analysis and Machine Intelligence*, vol. 20, no. 2, pp. 113–125, 1998.

[3] J. Tang and S. T. Acton, "Vessel boundary tracking for intravital microscopy via multiscale gradient vector flow snakes," *IEEE Transactions on Biomedical Engineering*, vol. 51, no. 2, pp. 316–324, February 2004.

[4] J. August and S.W. Zucker, "Sketches with curvature: the curve indicator random field and markov processes," *PAMI*, vol. 25, no. 4, pp. 387 – 400, April 2003.

[5] K. Raghupathy and T.W. Parks, "Improved curve tracing in images," *ICASSP 04*, vol. 3, no. 3, pp. 581–584, 2004.

[6] M.E. Martinez-Perez et al., "Segmentation of retinal blood vessels based on the second directional derivative and region growing," *Proceedings, ICIP '99*, vol. 2, 1999.

[7] J. Sethian, *Level Set Methods and Fast Marching Methods*, Cambridge Univ. Press, 1999.

[8] K. Kamath et al., "βiii-tubulin induces paclitaxel resistance in association with reduced effects on microtubule dynamic instability," *The Journal of Biological Chemistry*, vol. 280, no. 13, pp. 12902–12907, April 2005.